PASSIVATING OXIDE FILM AND GROWING CHARACTERISTICS OF ANODIC COATINGS ON ALUMINIUM ALLOYS

S. Feliu Jr*., Mª.J. Bartolomé, J.A. González, V. López and S. Feliu

Centro Nacional de Investigaciones Metalúrgicas, Avda. Gregorio del Amo, 8, 28040-Madrid, Spain

* Corresponding author: Fax:+34-91-534-7425-Tel: +34-91-553 89 00 (Ext 293)

E-mail address: sfeliu@cenim.csic.es(S. Feliu, Jr)

ABSTRACT

The paper studies some aspects of the behaviour of four aluminium alloys under chemical etching by sodium hydroxide solution and during their subsequent anodizing in sulphuric acid solution. A correspondence is seen between etching rate, thickness of the passivating oxide film and porosity of the anodic layer. The possibility of an influence on these properties of precipitates and micro-heterogeneities in the metallic surface is suggested.

Keywords: Aluminium alloys, passivating oxide film, porous anodic layer, XPS.

1. INTRODUCTION

During the last years investigators at CENIM laboratories have conducted a comprehensive study about the influence of second-phase particles on the characteristics and quality of the coatings produced by anodic oxidation of aluminium alloys and the filiform corrosion susceptibility of the lacquered surfaces in marine environment [1]. In the chemical/electrochemical treatments applied to the aluminium alloys a correspondence has been seen between thickness of the naturally formed oxide films on the tested alloys and a series of properties connected with the chemical attack and subsequent growing of porous anodic layers on their surface. It is the purpose of this paper to call attention to this finding, with particular reference to the following parameters: type of aluminium alloy, thickness of the natural oxide film formed on its surface, alkaline attack rate, porosity of the anodic coating, and efficiency of oxide production during anodizing. Special attention will be paid to the action of common factors in the mechanisms that determine the measured properties.

The present investigation has been made on the basis of four aluminium alloys selected with intent to give specific and substantial differences in the results. As we shall see along the work, the behaviour of these alloys falls clearly in two different groups, one formed by two binary alloys of the type Al-Cu and Al-Mg, containing comparatively large percentages of Cu and Mg, and the other formed by a ternary alloy of the type Al-Mg-Si and by 99.5 pure Al (Table 1). Anodized (and sealed) Al-Si-Mg, Al-Mg and commercially pure Al materials are widely used in architectural applications. They present different possibilities regarding the oxidation tendencies of the alloying elements and content and composition of second phase particles in the aluminium matrix. The highest alloying element concentration in the Al-Cu and Al-Mg systems tends to promote the occurrence of second phase particles. On the other hand, the Al-Cu alloy has the peculiarity of giving very defective oxide coatings [2-3]

2. EXPERIMENTAL

2.1. Materials

The materials investigated comprised the alloys (ISO designation): AlCu4MgSi, AlMg3, AlSi1MgMn and Al 99.5, which had been considered in previous investigations by the authors. These alloys are referred to throughout the work as Al-Cu, Al-Mg, Al-Si-Mg and pure Al, respectively (Table 1). The alloy referred to as pure Al (commercially pure Al) contains a total of about 0.5 wt% of other elements, mainly iron (0.290 wt% Fe) and silicon. Elemental compositions, determined in wet conditions, are detailed in Table 2.

The specimens were obtained from commercial rolled sheet.

2.2. Chemical and electrochemical treatments

The 100x50x1.5 mm specimens were degreased by submerging them for 5 minutes in an aqueous dissolution of phosphoric and chromic acids at concentrations of 15% vol. and 5% wt., respectively, at a temperature of 30-40ºC. They were then etched in an aqueous solution of 10% sodium hydroxide at 40-50 ºC for 5 min. and were desmutted by immersion for a few seconds in the aqueous solution of sulphuric acid and chromic acid. After each treatment the specimens were thoroughly rinsed in distillated water and dried with compressed air.

Anodic coatings were generated on specimens of the various alloys by submerging them in an aqueous dissolution of 18 g/l H_2SO_4 at 20ºC stirred with compressed air, through which a direct current density of 1.5 A/dm^2 was made to pass. The anodising times were variable, being chosen to produce coatings of approximately 5, 15 and 30 µm. Part of the specimens were then subjected to traditional hydrothermal sealing in boiling deionised water for 60 min, sufficiently long to achieve the sealing quality indices demanded by industry, even with the thickest coatings.

2.3. Tests

The XPS technique was used to analyse the elemental composition of the outer surface of the tested alloys. It was used also to determine the thickness of the very thin passivating oxide film present on the metal after chemical attack. For this calculation, use was made of the expression given by Roberts et al. [4]:

$$d_o\ (nm) = \lambda_o \sin\theta \ln [I_o \times \lambda_{metal} \times N_m) / (I_m \times \lambda_{oxide} \times N_o) + 1] \qquad (1)$$

where d_o is the thickness of the aluminium oxide layer (in nm); θ is the photoelectron exit angle; I_m and I_o are the intensities of the aluminium components in metallic state and as Al2p peak oxide; λ_{metal} and λ_{oxide} are the mean free path of photoelectrons in the substrate and the oxide layer; and N_m and N_o are the volume densities of aluminium atoms in metal and oxide.

Thickness of the anodic coatings (between about 5 to 35 μm) was determined instrumentally using equipment based on Foucault currents.

In order to examine the porous structure of the anodic films, sections parallel to the surface plane were prepared by ion thinning of the film previously separated from the metallic substrate by attack in a 0.05 M mercuric chloride solution. The thinned specimens were directly observed in a JEOL JEM 2010 transmission electron microscope.

Gravimetry was used to determine porosity of the anodic coatings and film formation efficiency. For this purpose, specimens were weighed immediately after surface preparation prior to anodizing, and after each of the subsequent processes of anodizing, sealing, and removal of the coatings in boiling phosphocromic mixtures [5].

Taking advantage of the extraordinary sensitivity of electrochemical impedance spectroscopy (EIS) to analyse the characteristics of the porous oxide layers [6], impedance diagrams of the anodized alloys were obtained.

3. RESULTS

XPS determinations. Tables 3 and 4 list the atomic percentages observed by XPS on the passivating films that cover the studied alloys after alkaline etching and on the subsequently formed anodic films, respectively. Only some of the elements determined in the bulk analysis have been detected on the outer surface of the alloys investigated. As can be seen, there are no significant differences among the various alloys. The O/Al atomic ratio for the passivating oxide films on the outer surface of the alloys (Table 3) coincides practically with the stoichiometric value of 1.50 for Al_2O_3. After anodizing, the O/Al ratio for the anodic coating (Table 4) is significantly higher as corresponding to a substantial hydroxide or oxy-hydroxide formation at the oxide surface.

On the other hand, column 3 of Table 5 lists passivating film thickness values after the chemical attack (i.e. values for the thin preexissting oxide film before anodizing).calculated from XPS data using equation (1).

Alkaline etching rate. Column 2 of Table 5 lists mass losses after 5 min of attack in 10wt% NaOH solution at 40ºC.

Mass gain values during anodizing. Figure 1 compares the mass gain values obtained during the anodizing of the four alloys investigated. Anodic oxidation of the metallic substrate gives rise to mass gains proportional to oxide thickness on the pure Al and Al-Mg and Al-Si-Mg alloys, and an abnormal mass loss in the special case of the Al-Cu alloy.

Film formation efficiency. The apparent film formation efficiency is measured by the coating ratio (CR) value (see later) and is represented in figure 2 as a function of the coating thickness. Column 5 of Table 5 lists CR values referred to layers of 25 μm thickness deduced from figure 2 (by extrapolation in the case of Al-Mg and Al-Cu alloys).

In calculating CR values, mass change determinations after anodizing (Fig. 1) and following the removal of the coating yield mass of the film formed. On the other hand, mass change determinations of the anodized specimen after removal of the coating and of the specimen prior to anodizing yield the mass of aluminium consumed.

Mass gain during sealing. Figure 3 plots the amount of water absorbed by the anodic coating when the anodized aluminium specimens are immersed in boiling water for 60 min.

The sealing mass gain is expected to increase with the porosity of the anodic oxide coating and may serve to calculate this parameter. In this work it has been considered that the mass gain obtained during sealing determines the volume occupied by the pores in the anodic films, accepting that they become saturated with water during the 60 minutes of immersion in boiling deionised water, while the total volume of the coating is estimated from its mass, accepting a density of 2.6 g/cm^3 for sealed oxides [7], or from its thickness determined instrumentally. Figure 4 plots the porosities estimated according to the latter procedure. Values in column 4 of Table 5 refer to a layer of 25 μm thickness.

Metallographic and EIS information. Examination by transmission electron microscopy has revealed a greater pore diameter on the Al-Mg alloy than on pure Al (Fig. 5). On the other hand, the Nyquist diagrams of figure 6 show marked differences in the behaviour of the anodized and just sealed four alloys.

4. DISCUSSION

Attention is drawn to the similarities in the ordering of the four tested alloys with regard to the studied properties, i.e. chemical etching rate, thickness of the passivating oxide film, porosity of the anodic coating and anodizing efficiency. This behaviour is shown in table 5. The existence of some correlations between the various parameters for the four alloys is expressed in figure 7. The roughly straight lines in the plots of etching rate against film thickness (A); film thickness against

porosity (B), and porosity against efficiency (C) seem to indicate that some kind of connection exists between these parameters. In general, the results suggest that common factors act on the mechanisms responsible for the measured values, as is discussed below.

4.1. Passivating film

The results in column 3 of Table 5 illustrates the significant influence of the type of alloy on the thickness of the naturally formed oxide film. It will be seen that film thickness values determined on the Al-Cu and Al-Mg alloys are 1.3-1.7 times greater than those for pure Al and the Al-Si-Mg alloy.

Like other metals, aluminium oxidises rapidly when exposed to the air or in an aqueous solution giving rise to the formation of passivating oxide films of just a few nanometres thickness. According to Mott and Cabrera's theory on the growth of very thin oxide films [8,9], the electric field associated with the presence of oxygen ions adsorbed on the metal surface is enormous at first, but quickly weakens as the film thickness grows, and after a few minutes the reaction virtually ceases. Although the passivating oxide films are of compact nature, defects of different nature are known to be widely present, as flaws due to the disturbing influence of second phase precipitates in the Al matrix, surface micro-irregularities, strains and lattice defects in the oxide layer [10, 11, 12].

A large amount of research has been published on the effect of imperfections in the naturally formed surface oxide on a number of properties of the aluminium alloys [13-21]. It appears to be possible that these imperfections may also have an effect on the thickness of the passivating film. According to literature an oxide film with a defective network structure grows on aluminium more readily than a non-defective one [22,23]. Also, to stressed and defective surface layers have been attributed the formation of thicker and less protective oxide films on stainless steel [24].

An explanation of the differences in film thickness observed in this work should perhaps take the above into account, assuming that a defective film produces enhanced film growth due to an easier diffusion of the reacting species.

4.2. Rate of attack during alkaline etching

The arrangement of the alloys according to their corrosion rate (metal mass losses in column 2 of Table 5) is similar to that observed for the oxide film thickness (column 3): i.e. substantially higher rates of chemical attack for the Al-Cu and Al-Mg alloys in comparison with the pure Al and Al-Si-Mg alloy. The correlation shown in figure 7, plot A, suggests that some factors involved in the process of alkaline etching have an influence also on the growth of the oxide film.

During the alkaline etching of aluminium the anodic reaction is supported by hydrogen evolution at cathodic sites on the metal surface [25-29]. As overpotential for hydrogen evolution on the surface of very pure (99.9999%) aluminium in alkaline solution is specially high, second phase particles in the aluminium alloys can facilitate this process by providing preferential sites for the cathodic reactions [25]; in this case, gas evolution on the cathodic particles proceeds parallel to gas evolution on the Al matrix surface contributing significantly to increase the corrosion rate. Electrochemical activity between second phase particles and the matrix depends on factors such as potential difference, proportion of surface occupied by the cathodic particles and their capability in depolarizing the cathodic reaction. All they will certainly have participated in the observed differences in the etching rate of the four tested alloys, although the details of their action in producing the results shown in column 2 of Table 5 are not known.

The anodic matrix dissolves strongly around second phase particles acting as local cathodes [13, 25]. Ditching of the matrix leads to physical separation of an appreciable fraction of particles from the alloy surface. Under the microscopy, this effect appears as depressions or cavities sharply cut out of the surrounding surface. Non-uniform growing of the oxide film is

predictable, which can generate highly localized stress development, distortion of the lattice and possible failures of the film. All these actions may render a more defective oxide and thereby facilitate diffusion and oxidation of aluminium.

Apart from the effect of second phase particles, recently it has been found [30-32] that NaOH etching of aluminium (as well as other dissolution treatments) exposes a large number of sub-micron cavities on its surface (see below). Hence there is the possibility that geometric micro-irregularities have played also a significant role in the formation of defective oxide films, adding their effect to that of the second phase particles.

On the basis of all above, it is suggested that the higher the rate of etching an alloy exhibits, the most defective, and thicker, oxide film is formed. This behaviour is reflected in figure 7 (plot A), in which case the thicker passivating oxide films determined on Al-Cu and Al-Mg (column 2 in table 5) would correspond to a larger amounts of defects in these films compared with pure Al and Al-Si-Mg.

4.3. Porosity of the anodic coating

Figure 4 (obtained from Fig. 3 and coating thickness) shows that porosity of the anodic films on the Al-Cu and Al-Mg alloys is substantially greater than with the pure Al and Al-Si-Mg alloy. With the exception of the value for pure Al, which does not differ very much from that for Al-Si-Mg (column 4 of Table 5), the same arrangement of the alloys first observed regarding thicknesses of the natural oxide films is appreciated now regarding porosity values of the subsequently formed anodic oxide coatings. This is clearly shown in figure 7 (plot B), where a linear relation between film thickness and porosity is apparent.

The porosity defined as the volume of pores per volume of the porous layer depends on the form, size and number of pores. In the case of oxide coatings constituted by an array of parallel

cylindrical pores, porosity is a function of their diameter and number. In figure 5 TEM offers a direct visualization of pore size, which is larger in the more porous coating. Closely connected with film porosity, impedance measurements show an important increase of the impedance in passing from Al-Cu and Al-Mg to pure Al and Al-Si-Mg alloys (Fig.6), reflecting less insulating (more porous) films on the two first alloys.

As is well known, the anodic oxide layer developed during anodizing in sulphuric acid consists of a thin relatively compact inner layer (barrier layer), and a thick, porous outer layer that grows on top of this. The nature of the barrier layer is similar to that of the passivating oxide film, which in certain way acts as a nucleation surface for it. Defects in the passivating film tend to be transferred to the barrier layer, whose role in the pore initiation process has been considered in several studies [3, 33-35]. In general, the porous anodic coating arises from the interplay of oxide formation at the metal-oxide interface and field-assisted oxide dissolution at the oxide-electrolyte interface [3, 33-36]. Pores tend to develop in the locally thinner regions of the barrier layer where the current is concentrated and field-assisted film dissolution increases. Even slight changes in the specific characteristics of the metallic surface seem to exert appreciable effect on the development and structural features of the anodic oxide coating. For example, investigations on the early stages of pore formation have indicated preferential pore development at grain boundaries and scratches [37,38].

Plot D in figure 7, between etching rate and porosity, results directly from plots A and B. In an attempt to explain the observed correlation, it poses a problem the fact that the population density of pores in the anodic layer is very much larger (about 10^5 times larger) than the reported population density of second phase particles on the aluminium alloys surface [25, 39], particles that, as has just been said (Section 4.2), play a crucial role in the etching process.

According to Herbert and co-authors [30-32], caustic etching of aluminium produces a defective subsurface layer containing a large number of nanometre-scale voids very near the metal-

oxide interface (possibly as a result of the condensation of metal vacancies generated by the dissolution process). These voids are transformed into surface cavities after a slight depth dissolution [35]. Since the number density of these voids (or cavities) is in the range of the number density of pores in the anodic layer, it should be not surprising that an influence of these voids on the initiation of the pores in the anodic coating may exist. In reality, we are ignorant of the exact mechanism by which pores and porosity develop in the anodic layer, but the idea that a certain correspondence exists between pore development sequences during film grows and preexisting features on the etched metal is an attractive hypothesis

4.4. Anodic coating formation efficiency

The process of conversion of metallic aluminium into a porous oxide layer during anodising in a sulphuric acid solution can be seen chiefly as a competition between two opposing reactions: (a) electrochemical growth of aluminium oxide, and (b) dissolution of the oxide by the electrolyte [3, 33, 36]. In certain cases there is also the possibility of a not negligible attack of the metallic aluminium to directly form soluble salts, reaction (c).

The so-called CR ratio between the weight of film formed during anodizing (in the paper, data in Fig. 1) and the weight of aluminium consumed gives a measure of film formation efficiency [3, 7, 34]. For comparison purposes, it is to be noted that CR is related to current efficiency, η (i.e. the fraction of the total charge passed through the cell used to form aluminium oxide), by $\eta = 0.53$ CR provided that oxygen gas evolution and chemical dissolution of aluminium do not occur to any significant extent, as it is usual [7]. As occurred with the other parameters, results in column 5 of Table 5 show a clear difference between the CR values determined for the Al-Cu and Al-Mg alloys, on the one hand, and for pure Al and Al-Si-Mg alloy on the other. The difference is specially marked with the greater coating thicknesses (Fig.2).

The lower CR values for the Al-Cu and Al-Mg alloys in comparison with those for the pure Al and Al-Si-Mg alloy can be explained as due to the higher dissolution rate of the porous oxide coatings formed on the first two alloys (i.e. to a greater effect of reaction b). As the results presented in figure 8 indicate, the oxide coatings on the Al-Cu and Al-Mg alloys exhibit the higher dissolution rates in the sulphuric acid bath (in the absence of current). The practically identical chemical composition for all the oxide coatings formed on the four tested alloys (Table 4) makes it unlikely a significant influence of the oxide composition on the results obtained. On the other hand, the roughly linear increase of mass losses with film thickness in figure 8 strongly suggests an effect of the surface area of the cylindrical pores. In this case, a proportionality between porosity and exposed area of the cylindrical pores can be expected if pore diameter varies while the number of pores per unit area is almost constant, as in figure 5.

So, the inverse relation shown in plot C of figure 7 (with efficiency decreasing as porosity increases) is foreseeable from the effect of porosity on reaction b, and the effect of this reaction on the denominator of the CR ratio.

5. CONCLUSIONS

1. A comparative study of commercially pure Al, Al-Mg-Si, Al-Mg and Al-Cu has revealed notable differences in the chemical attack rate in an alkaline solution and the thickness of the passivating oxide film that covers the metallic surface after etching. The highest attack rate and film thickness values have been obtained with the latter two alloys, which have the highest alloying element contents. It seems likely that the heterogeneous structure associated with second-phase particles has played a decisive role in the measured values.
2. In subsequent anodizing in sulphuric acid, the behaviour of the Al-Cu and Al-Mg alloys is also clearly differentiated from that of the pure Al and Al-Mg-Si, in terms of greater porosity of the anodic layer and a lower film formation efficiency (CR value). The results suggest a direct relationship between the preexisting oxide film thickness and the anodic layer porosity, and an inverse relationship with the CR value. In all cases it seems possible to sustain the hypothesis

of mechanisms influenced by a common factor, probably the presence of defects in the oxide film, which would be more abundant in the Al-Cu and Al-Mg alloys.

3. Everything seems to indicate that the defects in the natural oxide layers formed after alkaline etching determine the flaws in the barrier layer, and that the latter are transmitted to a greater or lesser degree to the porous layer during the anodising of the aluminium alloys.

Acknowledgements

This work was supported by the Comisión Interministerial de Ciencia y Tecnología (CICYT) of Spain within the framework of Project MAT2003-02217.

REFERENCES

1. J.A. González, V. López, E. Otero, S. Feliu, Jr, E. Escudero, M.J. Bartolomé, Project MAT2003-02217, “Effect of the size and concentration of intermetallic precipitates in the corrosion behaviour of anodized aluminium alloys”.
2. E. Huttunen-Saarivirta, T. Tiainen, Mater. Chem. Phys. 85 (2004) 383.
3. G.E. Thompson, G.C. Wood, in: J.C. Scully (ed.), Treatise on Materials Science and Technology, Vol. 23. Corrosion: Aqueous Processes and Passive Films, Academic Press, London, 1983, p.205.
4. A. Roberts, D. Engelberg, Y. Liu, G.E. Thompson and M.R. Alexander, Surf. Interface Anal. 33 (2002) 697.
5. UNE-EN standard 12373-2: 1999.
6. J.A. González, V. López, E.Otero, A. Bautista, J. Electrochem. Soc. 147 (2000) 984.
7. R.C. Spooner, J. Electrochem. Soc. 102 (1955) 156.
8. N. Cabrera, N.F. Mott, Rep. Progr. Phys. 12 (1948-49) 163.
9. J. Benard, Oxidation des Metaux, Gauthier-Villars, Paris 1962.
10. J.A. Richardson, G.C. Wood, Corros. Sci. 10 (1970) 313.
11. A. Barbucci, G. Bruzzone, M. Delucchi, M. Panizza, G. Cerisola, Intermetallics, 8 (2000) 305.
12. Y. Liu, P. Skeldon, G.E. Thompson, X. Zhou, H. Habazaki, K. Shimizu, Corros. Sci. 42 (2001) 2349.
13. R.P. Wei, Chin-Min-Liao, Ming Gao, Metall. Mater. Trans. A, 29A (1998) 1153.
14. G.S. Chen, M.Gao, R.P. Wei, Corrosion, 52 (1996) 8.
15. P. Campestrini, E.P.M. Van Westing, H.W. Rooijen, J.H.W. Wit, Corros. Sci. 42 (2000) 1853.
16. F. Andreatta, H. Terryn, J.H.W. Wit, Electrochim. Acta 49 (2004) 2851.
17. P. Skeldon, S.X. Zhou, G.E. Thompson, G.C. Wood, H. Habazaki, K. Shimizu, Corrosion 55 (1999) 561.
18. H. Leth-Olsen, K. Nisancioglu, Corros. Sci. 40 (1998) 1179.
19. D. Chidambaram, C.R. Clayton, G.P. Halada, N.W. Kendig, J. Electrochem. Soc. 151 (2004) B 605.

20. C.M.A. Brett, Corros. Sci. 33 (1992) 203.
21. O. Lunder, B. Olsen, K. Nisancioglu, Int. J. Adhesion Adhesives. 22 (2002) 143.
22. C. Ocal, B. Basurco, S. Ferrer, Surf. Sci. 157 (1985) 233.
23. N.A. Braaten, J.K. Grepstad, S. Raaen, Surf. Sci. 222 (1989) 499.
24. A.L. Johnson, D. Parsons, J. Manzerova, D.L. Perry, D. Koury, B. Hosterman, J.W. Farley, J. Nucl. Mater. 328 (2004) 88.
25. E.V. Koroleva, G.E. Thompson, G. Hollrigl, M. Bloeck, Corros. Sci. 41 (1999) 1475.
26. K.C. Emregül, A. Abbas Aksüt, Corros. Sci. 42 (2000) 2051.
27. D. Chu, R.F. Savinell, Electrochim. Acta. 36 (1991) 1631
28. M.L. Doche, J.J. Rameau, R. Durand, F. Novel-Cattin, Corros. Sci. 41 (1999) 805.
29. K. Nisancioglu, J. Electrochem. Soc. 137 (1990) 69.
30. K.R. Hebert, H. Wu, T. Gessmann, K.G. Lynn, J. Electrochem. Soc. 148 (2001) B92.
31. T. Martin, K.R. Hebert, J. Electrochem. Soc. 148 (2001) B101.
32. R. Huang, K.R. Hebert, T. Gessmann, K.G. Lynn, J. Electrochem. Soc. 151 (2004) B227.
33. G.C. Wood in J.W. Diggle, Marcel Dekker (ed), Oxides and Oxide Films, Vol. 2, New York, 1972, p.167.
34. G.C. Wood, J.P. O´Sullivan, Electrochim. Acta, 15 (1970) 1865.
35. R. Huang, K.R. Hebert, L.S. Chumbley, J. Electrochem. Soc. 151 (2004) B379.
36. S. Wernick, R. Pinner, P.G. Sheasby, in ASM International (ed), The Surface Treatment and Finishing of Aluminium and its Alloys, Vol. 1.Finishing publications, Ltd., Teddington, Middlesex, England, 1987, p. 289.
37. L.E. Fratila-Apachitei, F.D. Tichelar, G.E. Thompson, H. Terryn, P. Skeldon, J. Duszcyk, L. Katgerman, Electrochim. Acta, 49 (2004) 3169.
38. O. Jessensky, F. Müller, U. Gösele, J. Electrochem. Soc. 145 (1998) 3735.
39. A. Afseth, J.H. Nordlien, G.M. Scaman, K. Nisancioglu, Corros. Sci. 43 (2001) 2359

Figure Captions

Figure. 1. Mass gain during anodising as a function of alloy type and anodic film thickness.

Figure. 2. Coating ratio as a function of alloy type and anodic film thickness.

Figure. 3. Mass gain during sealing as a function of alloy type and anodic film thickness.

Figure. 4. Anodic film porosity as a function of alloy type and anodic film thickness.

Figure. 5. Transmission electron micrographs of anodic films developed on pure Al (top) and on the Al-Mg alloy (bottom).Scale dimensions are 20 nm.

Figure. 6. Impedance diagrams for the anodized and just sealed tested materials. Note the change of scale in passing from the Al-Si-Mg and pure Al to the Al-Mg and Al-Cu alloys.

Figure. 7. Plots of (A) film thickness against etching rate (i.e. metal losses in 5 min.); (B) porosity against film thickness; (C) porosity against efficiency; and (D) porosity against etching rate. Results from data in Table 5.

Figure. 8. Mass loss of unsealed anodic films on various alloys held for one hour in the anodising bath in the absence of current, as a function of film thickness.

Table Captions

Table 1. Tested alloys

Table 2. Chemical composition of aluminium alloys (weight percentage).

Table 3. Atomic percentages observed by XPS on the outer surface of the various alloys after etching prior to anodising and 10 minutes of Ar ion sputtering.

Table 4. Atomic percentages observed by XPS on the outer surface of the various alloys after the anodising operation

Table 5. Metal mass loss values after 5 min of attack, passivating oxide film thickness, anodic layer porosity, and coating ratio (the latter values for layers of 25 μm thickness) of the four tested alloys.

TABLES

Table 1. Tested alloys.

ISO designation	Designation in the paper
AlCu4MgSi	Al-Cu
AlMg3	Al-Mg
AlSi1MgMn	Al-Si-Mg
Al 99.5	Pure Al

Table 2. Chemical composition of aluminium alloys (weight percentage).

SPECIMEN	Si	Fe	Cu	Mn	Mg	Cr	Zn	TI
pure Al	0.080	0.290	0.003	0.003	0.006	----	0.040	0.012
Al-Cu	0.370	0.340	4.040	0.630	0.600	0.010	0.050	0.050
Al-Si-Mg	0.880	0.360	0.040	0.470	0.800	0.003	0.040	0.060
Al-Mg	0.090	0.260	0.001	0.110	2.900	---	0.022	0.004

Table 3. Atomic percentages observed by XPS on the outer surface of the various alloys after etching prior to anodising and 10 minutes of Ar ion sputtering.

SPECIMEN	% O	% Al	% Mg	% Cu	O/Al
Pure Al	60	40	0	0	1.5
Al-Cu	60	40	0	1	1.5
Al-Si-Mg	61	39	0	0	1.56
Al-Mg	58	38	0	0	1.53

Table 4. Atomic percentages observed by XPS on the outer surface of the various alloys after the anodising operation.

SPECIMEN	% O	% Al	% S	O/Al
Pure Al	66	32	2	2.1
Al-Cu	66	32	2	2.1
Al-Si-Mg	64	33	3	1.9
Al-Mg	64	34	2	1.9

Table 5. Metal mass loss values after 5 min of attack, passivating oxide film thickness, anodic layer porosity, and coating ratio (the latter values for layers of 25 μm thickness) of the four tested alloys.

ALLOY	METAL MASS LOSS (mg/cm^2)	OXIDE FILM THICKNESS (nm)	APPARENT ANODIC LAYER POROSITY (%)	COATING RATIO
Pure Al	2.05	2.2	17	1.3
Al-Si-Mg	2.15	2.3	13	1.4
Al-Mg	2.85	3.0	25	1.1
Al-Cu	3.31	3.8	38	0.5

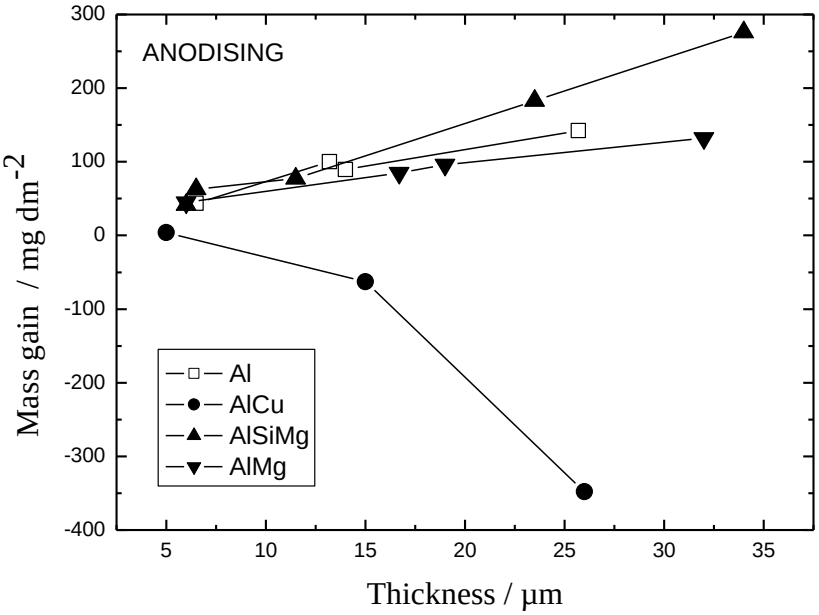

Fig. 1. Mass gain during anodising as a function of alloy type and anodic film thickness.

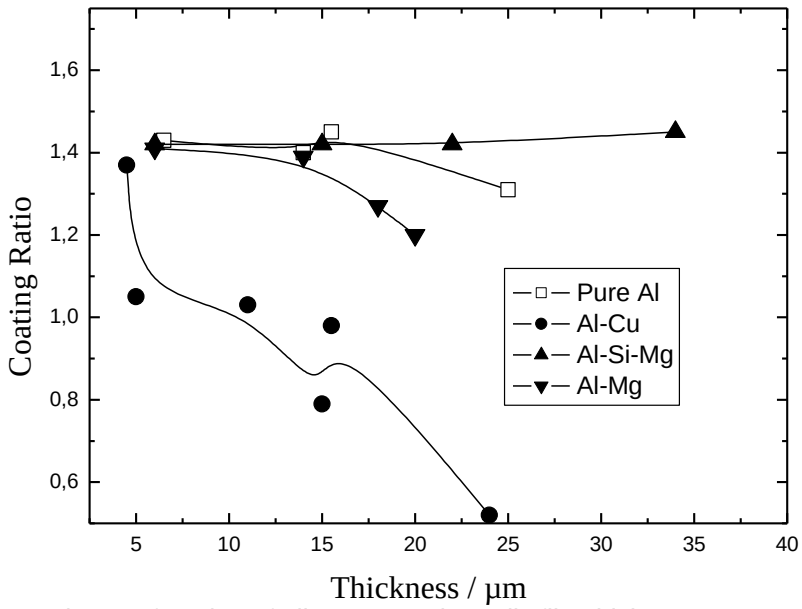

Fig. 2. Coating ratio as a function of alloy type and anodic film thickness.

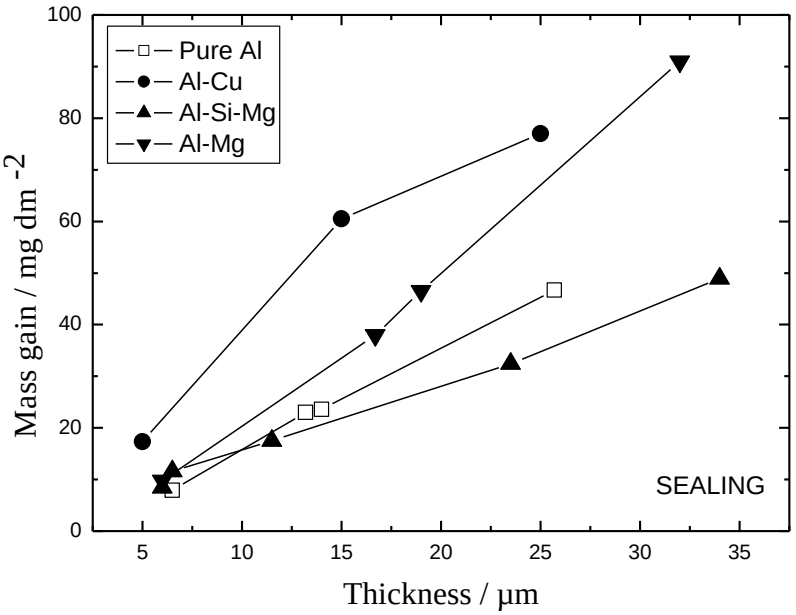

Fig. 3. Mass gain during sealing as a function of alloy type and anodic film thickness.

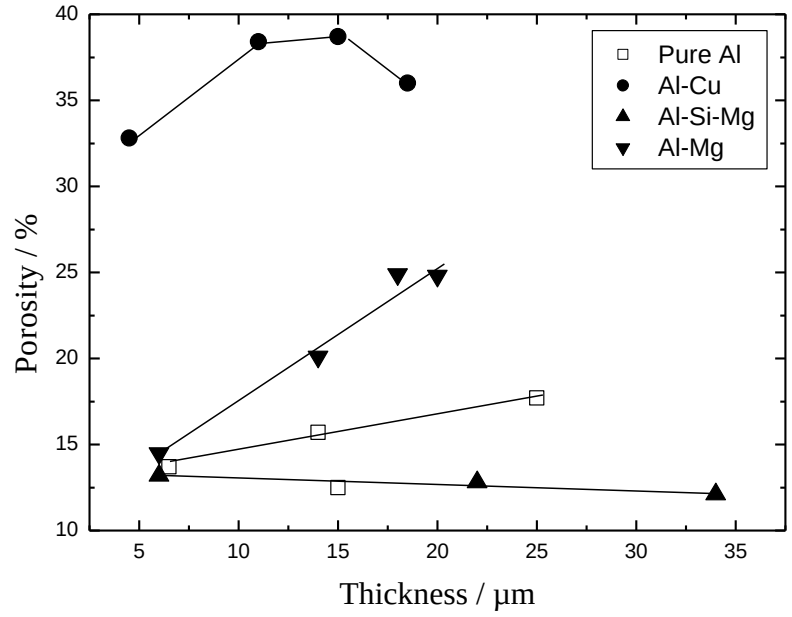

Fig. 4. Anodic film porosity as a function of alloy type and anodic film thickness.

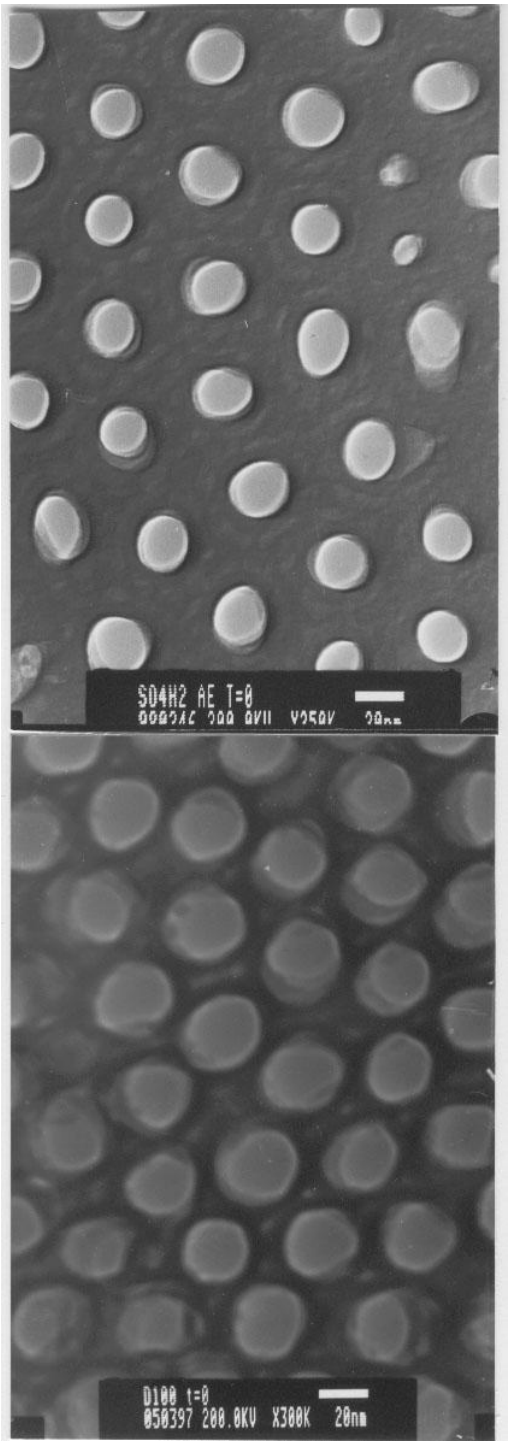

Fig. 5. Transmission electron micrographs of anodic films developed on pure Al (top) and on the Al-Mg alloy (bottom).Scale dimensions are 20 nm.

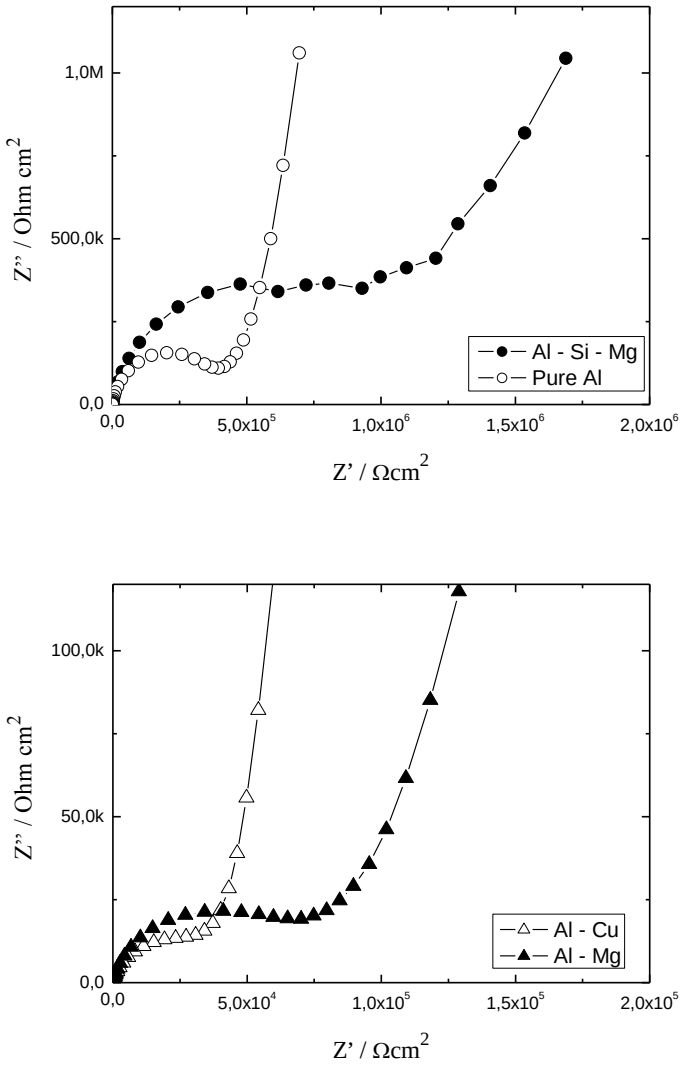

Fig. 6. Impedance diagrams for the anodized and just sealed tested materials. Note the change of scale in passing from the A-Si-Mg and pure Al to the Al-Mg and Al-Cu alloys.

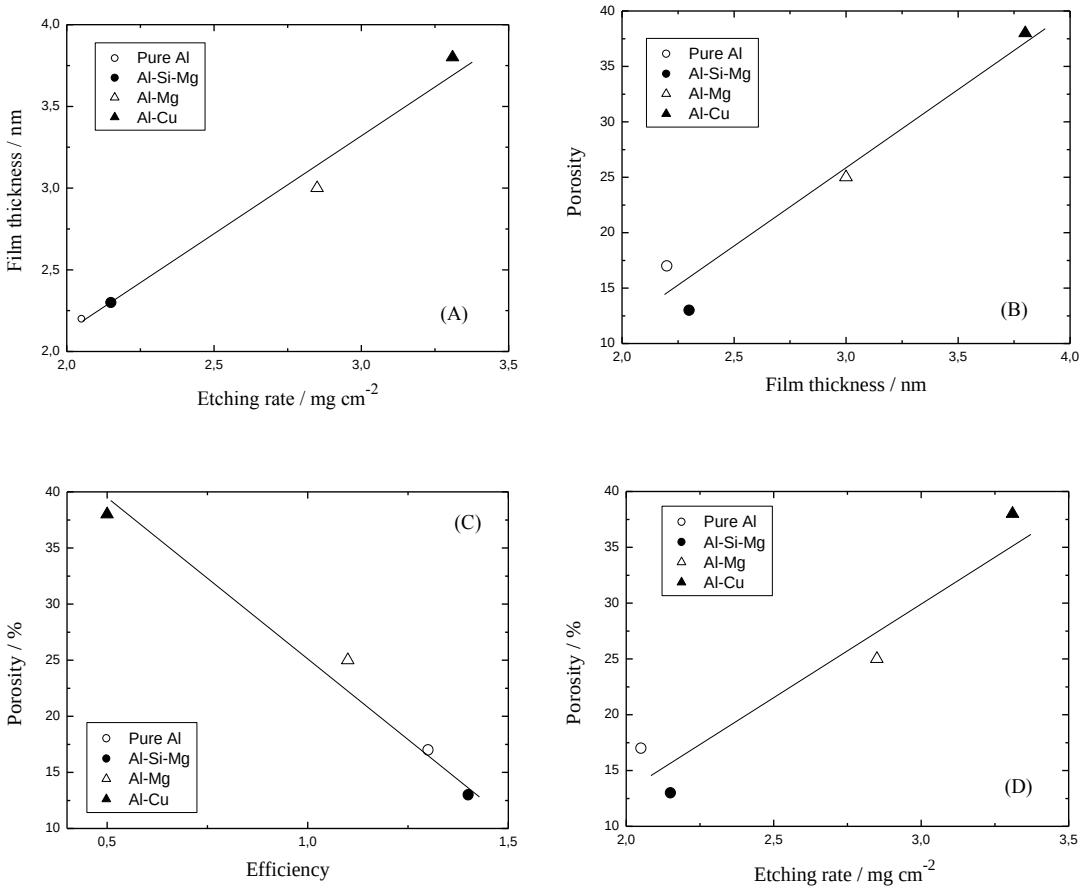

Fig. 7. Plots of (A) film thickness against etching rate (i.e. metal losses in 5 min.); (B) porosity against film thickness; (C) porosity against efficiency; and (D) porosity against etching rate. Results from data in Table 5.

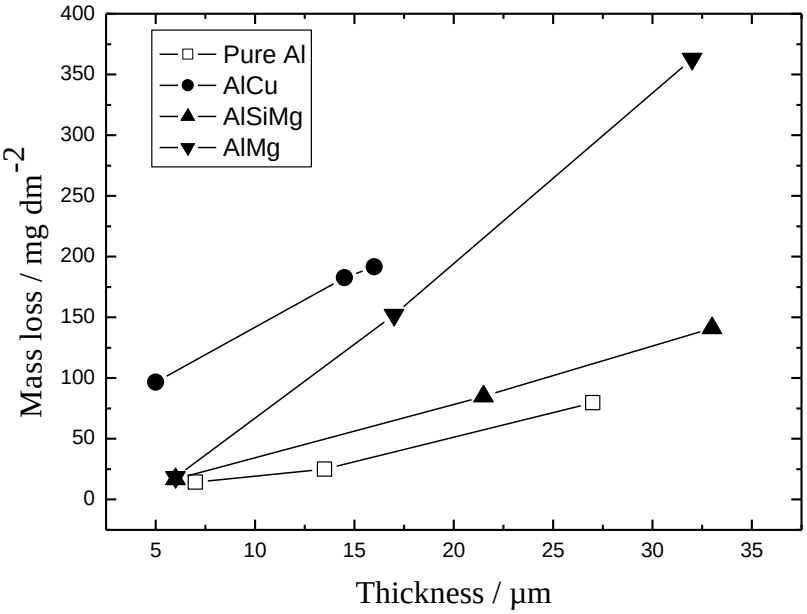

Fig. 8. Mass loss of unsealed anodic films on various alloys held for one hour in the anodising bath in the absence of current, as a function of film thickness.